12th International Symposium on Turbulence and Shear Flow Phenomena (TSFP12)
Osaka, Japan (Online), July 19-22, 2022

THE STRUCTURE OF TURBULENT CHANNEL FLOW OVER RATCHET-TYPE ROUGHNESS

Angela Busse
James Watt School of Engineering
University of Glasgow
Glasgow, United Kingdom, G12 8QQ
angela.busse@glasgow.ac.uk

Oleksandr Zhdanov
James Watt School of Engineering
University of Glasgow
Glasgow, United Kingdom, G12 8QQ
oleksandr.zhdanov@glasgow.ac.uk

ABSTRACT

Ratchet surfaces are a form of regular two-dimensional spanwise bar roughness where the bars have a scalene triangular cross-section. The structure of turbulent channel flow over ratchet surfaces is investigated using direct numerical simulations at $Re_\tau = 395$ for a set of five ratchet surfaces with ratchet lengths from $2k$ to $16k$, where k is the ratchet height, in windward and leeward orientation giving a total of ten cases. The focus of this paper is the turbulent kinetic energy and the Reynolds stress anisotropy measured at the mid-cavity and the ratchet crest location. Both show strong dependence on the ratchet length and orientation. Visualisations of the instantaneous wall-normal vorticity field show that the near-wall turbulence activity is strongest at the mid-cavity location for ratchets in leeward orientation, whereas the highest turbulence activity is observed upstream of the roughness crests for ratchets in windward orientation.

INTRODUCTION

The effect of a rough surface on a wall-bounded turbulent flow strongly depends not only on the roughness height but also on the roughness topography. One of the key topographical parameters in this context is the effective slope of a rough surface (Chung *et al.*, 2021), which is defined as (Napoli *et al.*, 2008)

$$ES = \frac{1}{A}\int \left| \frac{\partial h(x,y)}{\partial x} \right| dxdy \qquad (1)$$

where $h(x,y)$ is the height of the surface as a function of the streamwise (x) and the spanwise (y) coordinate and A is the planform area of the heightmap.

One of the weaknesses of the effective slope parameter is that, by definition, it is insensitive to the orientation of the rough surface: upslope sections, where $\partial h(x,y)/\partial x > 0$, make the same absolute contribution to ES as downslope sections, where $\partial h(x,y)/\partial x < 0$, although wall-bounded turbulent flows tend to interact much more strongly with the windward sides of roughness features than with their leeward sides. In most cases, this insensitivity to the sign of the slope is not relevant, since for the majority of rough surfaces the probability density function of $\partial h(x,y)/\partial x$ is not skewed, and therefore no significant orientation dependency is expected.

However, there are rough surfaces where a significant imbalance in the slope distribution can be observed. For example, geomorphical forms such as transverse sand dunes typically have a low windward slope and a high leeward slope which is a result of their formation processes (Gao *et al.*, 2015). Further examples from a geophysical context, where skewed slope distributions can emerge, include sand ripples and some types of ocean waves. Other roughness generation processes may also produce orientation dependent roughness. For example, some icing processes experienced by aircraft (e.g., run-back icing) can result in roughness forms that have higher windward slopes than leeward slopes (Whalen *et al.*, 2007).

Ratchet-type roughness is an idealised two-dimensional form of roughness that is comprised of transverse bars with scalene triangular cross-section. By varying the relative slope of the leeward versus the windward side of the triangle, rough surfaces can be constructed that have identical effective slope but different windward and leeward slopes. Using direct numerical simulations of channel flow we showed that the roughness function ΔU^+ of ratchets in high windward slope orientation is significantly higher than for otherwise identical ratchet surfaces in low windward slope orientation (Busse & Zhdanov, 2021). Previously, Jiang *et al.* (2018) demonstrated for turbulent convection over ratchet roughness that large-scale convective structures are strongly influenced by the orientation of ratchet surfaces. The present investigation therefore aims to determine whether structures in turbulent channel flow are also strongly influenced by ratchet orientation. To this end, the structure of turbulent channel flow over ratchet-type roughness is investigated from both an Eulerian and a Lagrangian viewpoint.

ℓ	$2k$	$2k$	$4k$	$4k$	$8k$	$8k$	$12k$	$12k$	$16k$	$16k$
a/ℓ	$1/8$	$7/8$	$1/8$	$7/8$	$1/8$	$7/8$	$1/8$	$7/8$	$1/8$	$7/8$
orientation	ww	lw	ww	lw	ww	lw	ww	lw	ww	lw
ES	1	1	0.5	0.5	0.25	0.25	0.167	0.167	0.125	0.125
$Ssk_{\partial h/\partial x}$	$+2.3$	-2.3	$+2.3$	-2.3	$+2.3$	-2.3	$+2.3$	-2.3	$+2.3$	-2.3

Table 1. Key geometrical and topographical parameters of the ratchet surface: ℓ - base length of the triangular cross-section; a - x-coordinate of apex; orientation of high slope section (ww - windward; lw - leeward); ES - effective slope; $Ssk_{\partial h/\partial x}$ - skewness of streamwise slope distribution.

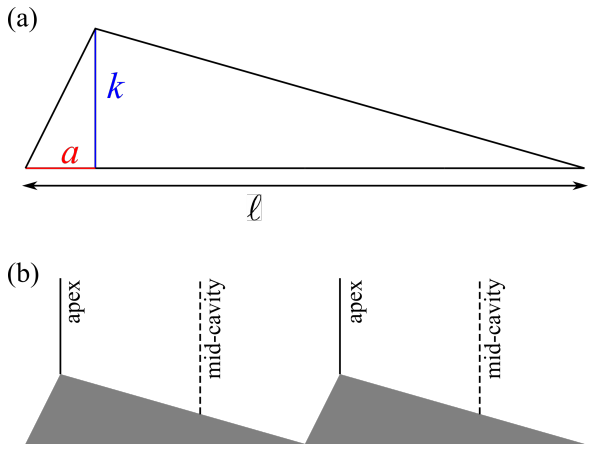

Figure 1. (a) Schematic cross-section of a triangular bar. k is the roughness height, ℓ is the length of the bar. By moving the apex location, a, a high windward slope or a high leeward slope can be achieved. The mean flow direction is from left to right. (b) Measurement locations for statistics: apex location (solid line) and mid-cavity location (dashed line); statistics are phase averaged over repeating units.

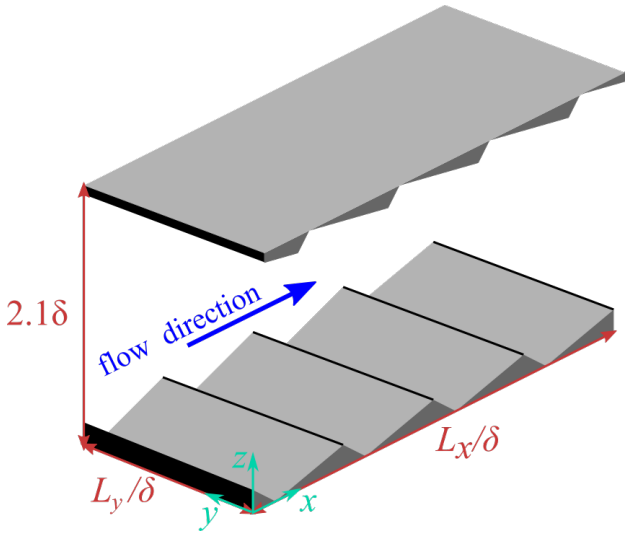

Figure 2. Schematic illustration of the computational domain (not to scale). The ratchet roughness is applied to both channel walls. On the upper wall, the pattern is shifted by $\ell/2$ in the streamwise direction. A ratchet case in leeward orientation is shown.

METHODOLOGY

Ten different ratchet surfaces were constructed using bars of different triangular cross-sections (see schematic shown in Figure 1(a)). In all cases, the height of the triangles was set to $k = 0.1\delta$, where δ is the mean channel half-height. The base size of the triangle, ℓ, was varied from 0.2δ to 1.6δ. The entire surface was covered by the triangular bars, i.e., the plan solidity, λ_p, is unity for all cases. For roughness composed of triangular transverse bars at $\lambda_p = 1$ the effective slope is given by $(2k)/\ell$, i.e., for the present cases ES was varied from 1 to 0.125 as ℓ was increased. An imbalance between the slopes of the two sides of the triangle interacting with the flow was introduced by positioning the x-coordinate of apex of the triangle, a, at $1/8\ell$ to create triangles with high windward and low leeward slope (windward oriented ratchet). To create equivalent leeward oriented ratchets, a was positioned at $7/8\ell$, i.e., effectively mirroring the triangle with respect to the vertical axis. Table 1 gives an overview of key topographical parameters of the surfaces. Due to the simple triangular form of the present surfaces, all of them have the same height distribution, and the root mean square roughness height and skewness of the height distribution are identical for all cases ($Sq = k/(2\sqrt{3})$, $Ssk = 0$). The skewness of the streamwise slope distribution $Ssk_{\partial h/\partial x}$ is positive for ratchets in windward orientation and negative in leeward orientation ($Ssk_{\partial h/\partial x} = (\ell - 2a)/\sqrt{a(\ell - a)}$ for triangular transverse bars at $\lambda_p = 1$).

For each case, a direct numerical simulation of incompressible turbulent channel flow was conducted at $Re_\tau = 395$ using the code iIMB (Busse *et al.*, 2015) which uses an iterative version of the embedded boundary method of Yang & Balaras (2006) to resolve the roughness. The ratchet surfaces were applied to both walls of the channel and the flow was driven by a constant mean streamwise pressure gradient. A schematic illustration of the domain is shown in Figure 2. The wall reference location was set to the roughness mean plane, i.e., the total wall-normal extent of the simulation domain was 2.1δ. For cases with $\ell = 2^n k$ the domain size was set to 6.4δ in the streamwise and 3.2δ in the spanwise direction (see Table 2). For the case $\ell = 12k$ the domain size was increased to 7.2δ in the streamwise direction to fit an integer number of transverse triangular bars into the domain. Uniform grid spacing was applied in the streamwise and spanwise direction, using $\Delta y^+ = 4.94$ and $\Delta x^+ \leq 4.94$. For short ratchets, the streamwise grid spacing was reduced to keep a minimum of 128 grid points per ratchet. In the wall-normal direction, uniform grid spacing was applied across the height of the ratchet $\Delta z^+_{\text{min}} = 0.667$ and the grid was gradually stretched above attaining $\Delta z^+_{\text{max}} = 4.22$ at the channel centre.

RESULTS

Local statistics for the turbulent kinetic energy measured at the apex location and at the mid-cavity location are shown

Table 2. Simulation parameters for the direct numerical simulations. L_x - domain size in streamwise direction; L_y - domain size in spanwise direction; L_z - domain size in wall-normal direction; $N_x \times N_y \times N_z$ - grid size; Δx^+ - grid spacing in streamwise direction; Δy^+ - grid spacing in spanwise direction; $\Delta z^+_{\mathrm{min}}$ - minimum wall-normal grid spacing; $\Delta z^+_{\mathrm{max}}$ - maximum wall-normal grid spacing.

	L_x/δ	L_y/δ	L_z/δ	$N_x \times N_y \times N_z$	Δx^+	Δy^+	$\Delta z^+_{\mathrm{min}}$	$\Delta z^+_{\mathrm{max}}$
$\ell = 2k$	6.4	3.2	2.1	$4096 \times 256 \times 432$	0.67	4.94	0.67	4.22
$\ell = 4k$	6.4	3.2	2.1	$2048 \times 256 \times 432$	1.23	4.94	0.67	4.22
$\ell = 8k$	6.4	3.2	2.1	$1024 \times 256 \times 432$	2.47	4.94	0.67	4.22
$\ell = 12k$	7.2	3.2	2.1	$1152 \times 256 \times 432$	2.47	4.94	0.67	4.22
$\ell = 16k$	6.4	3.2	2.1	$1024 \times 256 \times 432$	2.47	4.94	0.67	4.22
smooth	8.0	4.0	2.0	$640 \times 320 \times 360$	4.94	4.94	0.50	3.98

in Figure 3. Closely above the ratchets, the streamwise measurement location has the strongest effect for flow over long ratchets ($\ell \geq 8k$) in leeward orientation – the maximum observed for the turbulent kinetic energy profile is significantly higher when measured at the mid-cavity location compared to the equivalent measurements taken at the apex location. The opposite behaviour can be observed for ratchets in windward orientation. Here, for long ratchets significantly higher levels of turbulent kinetic energy can be observed above the apex location compared to the mid-cavity location.

The turbulent kinetic energy profiles for the shorter ratchets show a good collapse on the smooth-wall turbulent kinetic energy profiles for $z/\delta \gtrapprox 0.2$. For long ratchets ($\ell \geq 8k$), the differences in the turbulent kinetic energy profiles extend further into the flow. This deviation from the smooth-wall behaviour tends to be more pronounced for ratchets in windward orientation and for the mid-cavity location.

The Reynolds stress anisotropy measured at the apex and the mid-cavity locations was analysed using the invariants ξ and η which are derived from the anisotropy tensor b_{ij} (Pope, 2000)

$$6\eta^2 = b_{ij}b_{ji}, \tag{2}$$

$$6\xi^3 = b_{ij}b_{jk}b_{ki}. \tag{3}$$

The anisotropic invariant maps of η plotted versus ξ are shown in Figure 4 based on the Reynolds stress profiles measured at the apex location (see Figure 4 (a,b)) and at the mid-cavity location (see Figure 4 (c,d)). When the profiles are sampled at the apex location, in all cases the trajectories first approach the left boundary of the Lumley triangle, i.e., the Reynolds stress ellipsoid attains an approximately axisymmetric, oblate spheroid shape ('disk'-like turbulence). A similar behaviour was reported for roughness comprised of transverse square bars (Ashrafian & Andersson, 2006).

Disk-like turbulence is also observed within the cavities of the surface, however, above the reference crest location (indicated by the square symbols on the maps) the trajectories corresponding to the mid-cavity location remain close to the right side of the triangle and follow the reference smooth-wall case ('rod'-like turbulence). For short ratchets, there are no significant differences between trajectories for the ratchet roughness in leeward and in windward orientation at locations above $z/\delta \approx 0.15$.

For long ratchets, the windward oriented cases experience at the mid-cavity location a stronger tendency towards two-dimensional turbulence above the roughness and the differences between the trajectories for surfaces in windward and in leeward orientations extend significantly further into the flow. This is also evident from the profiles of the anisotropy function $F = 1 - 27\eta^2 + 54\xi^3$ ($F = 1$ for three-dimensional and $F = 0$ for two-dimensional turbulence), where lower levels of isotropy can be observed for long ratchets in windward orientation in the outer part of the profile up to the channel centre whereas the leeward oriented cases show a good collapse on the smooth-wall case for $z/\delta \gtrapprox 0.2$ for all ratchet lengths.

Figure 5 shows a visualisation of the wall-normal component of the instantaneous vorticity field closely above the ratchets at a distance of approximately 12 wall units above the roughness crests. Ratchet length and orientation have a strong effect on how the structure of the vorticity field is affected by the roughness. With decreasing ratchet length the organisation of the ω_z contours is increasingly reduced. The reduction in the organisation of structures in the instantaneous wall-normal vorticity field is in line with observations for transverse bar roughness (Ashrafian & Andersson, 2006; Orlandi & Leonardi, 2009).

For ratchets in leeward orientation, the strongest disruption of structures can be observed at the mid-cavity locations, whereas for ratchets in windward orientation, the strongest interaction between the vorticity field and the ratchets can be observed just upstream of the crest locations. The orientation-dependent differences are most obvious for the longest ratchets with $\ell = 16k$ and become less pronounced for the shorter ratchets. This is in line with the observations for the turbulent kinetic energy profiles, which show elevated levels at the crest location for ratchets in windward orientation and elevated levels at the mid-cavity location for ratchets in leeward orientation. This dependency of turbulent kinetic energy levels on the measurement location is also most strongly developed for the longest ratchets.

CONCLUSIONS

The structure of turbulence over ratchet-type roughness has been analysed using local phase- and time-averaged profiles of the turbulent kinetic energy and the invariant maps of the anisotropy tensor. Both ratchet length and ratchet orientation influence the local profiles of the turbulent kinetic energy and the anisotropic invariant maps. Flow visualisations of the instantaneous wall-normal vorticity field show that the streamwise locations of elevated turbulence activity are strongly influenced by the ratchet orientation. The influence of ratchet length and orientation on further statistics, such as ejections and sweeps, the wall-normal transport velocity of

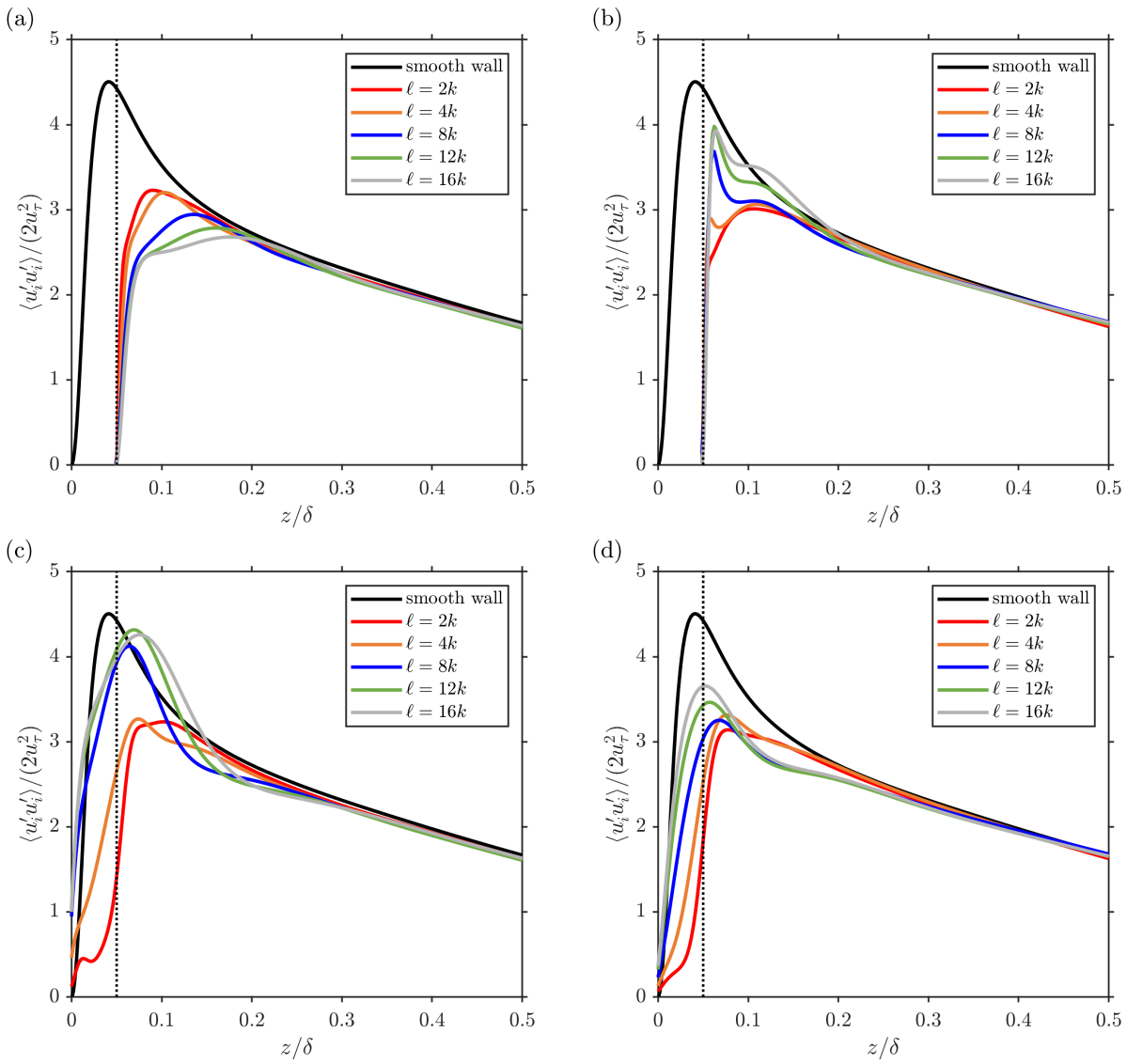

Figure 3. Turbulent kinetic energy profiles sampled at the apex location (a,b) and the mid-cavity (c,d) location for surfaces in leeward orientation (a,c) and in windward orientation (b,d). Smooth wall data is shown for comparison. The vertical dotted line indicates the apex height.

the turbulent kinetic energy, and tracer particle statistics will be considered in the next stage of this study.

ACKNOWLEDGEMENTS

This work used the Cirrus UK National Tier-2 HPC Service at EPCC (http://www.cirrus.ac.uk) funded by the University of Edinburgh and the Engineering and Physical Sciences Research Council (EP/P020267/1). A.B. gratefully acknowledges support via a Leverhulme Trust Research Fellowship for this work.

REFERENCES

Ashrafian, A. & Andersson, H. I. 2006 The structure of turbulence in a rod-roughened channel. *International Journal of Heat and Fluid Flow* **27**, 65–79.

Busse, A., Lützner, M. & Sandham, N. D. 2015 Direct numerical simulation of turbulent flow over a rough surface based on a surface scan. *Computers & Fluids* **116**, 129–147.

Busse, A. & Zhdanov, O. 2021 Turbulent channel flow over ratchet-type roughness. In *Proceedings of the 13th International ERCOFTAC symposium on Engineering, Turbulence, Modelling and Measurements (ETMM 13), Rhodes, Greece, 15-17 Sep 2021*.

Chung, D., Hutchins, N., Schultz, M. P. & Flack, K. A. 2021 Predicting the drag of rough surfaces. *Annual Review of Fluid Mechanics* **53**, 439–471.

Gao, X., Narteau, C. & Rozier, O. 2015 Development and steady states of transverse dunes: A numerical analysis of dune pattern coarsening and giant dunes. *Journal of Geophysical Research: Earth Surface* **120** (10), 2200–2219.

Jiang, H., Zhu, X., Mathai, V., Verzicco, R., Lohse, D. & Sun, C. 2018 Controlling heat transport and flow structures in thermal turbulence using ratchet surfaces. *Physical Review Letters* **120** (4), 044501.

Napoli, E., Armenio, V. & De Marchis, M. 2008 The effect of the slope of irregularly distributed roughness elements on turbulent wall-bounded flows. *Journal of Fluid Mechanics*

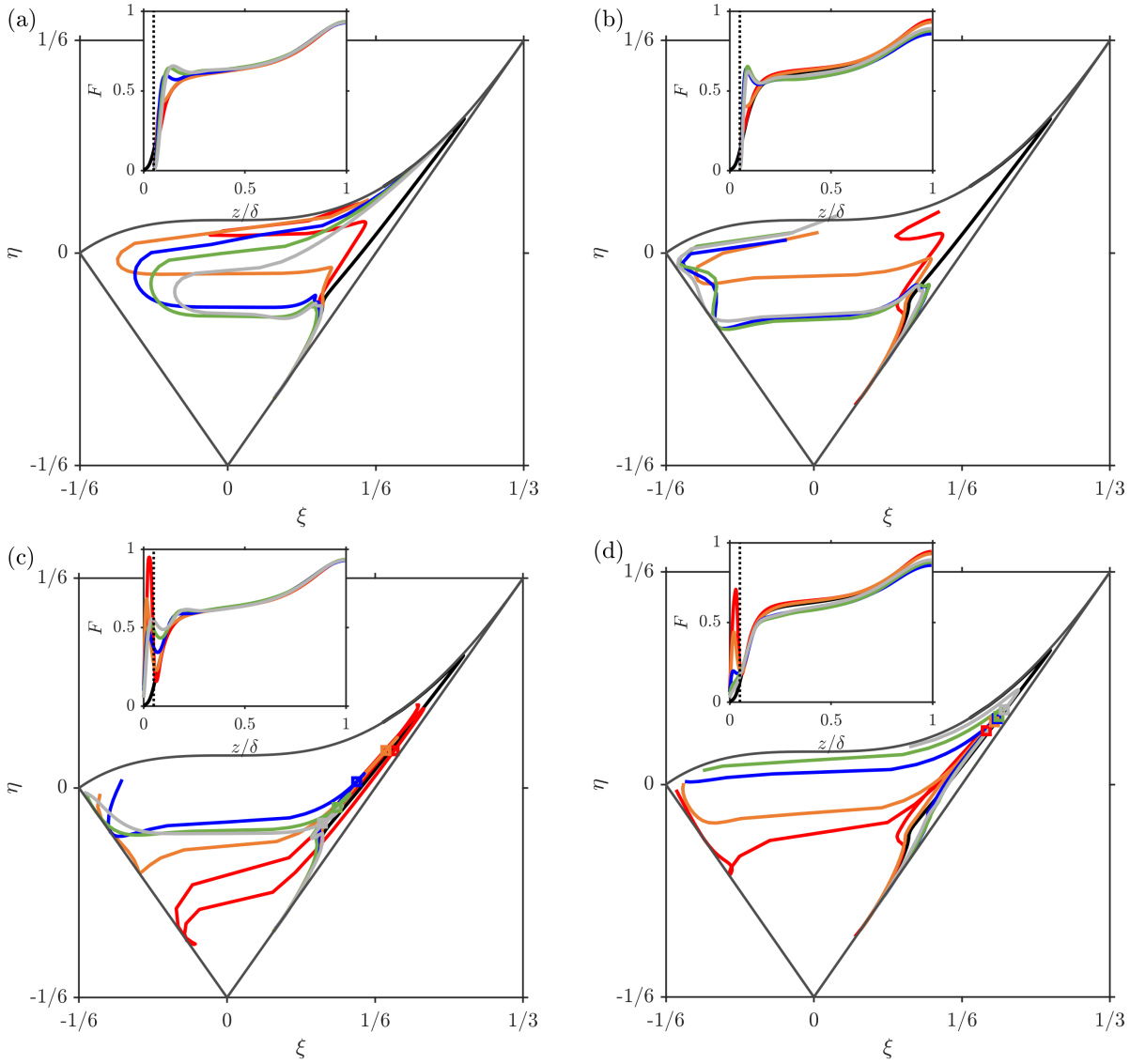

Figure 4. Anisotropic invariant maps (AIM) based on Reynolds stresses measured at the apex location (a,b) and at the mid-cavity location (c,d) for ratchets in leeward (a,c) and windward (b,d) orientation. For the trajectories based on Reynolds stresses measured at the mid-cavity location, the wall-normal location corresponding to the ratchet height is indicated using squares. The inset panels show the corresponding profiles of the anisotropy function F. Lines styles as in Figure 1.

613, 385–394.

Orlandi, P. & Leonardi, S. 2009 DNS of turbulent channel flows with two- and three-dimensional roughness. *Journal of Turbulence* **7**, 53.

Pope, S. B. 2000 *Turbulent Flows*. Cambridge University Press.

Whalen, E. A., Broeren, A. P. & Bragg, M. B. 2007 Characteristics of runback ice accretions and their aerodynamic effects. *Tech. Rep.* DOT/FAA/AR-07/16. U.S. Department of Transportation, Federal Aviation Administration.

Yang, J. & Balaras, E. 2006 An embedded-boundary formulation for large-eddy simulation of turbulent flows interacting with moving boundaries. *Journal of Computational Physics* **215** (1), 12–40.

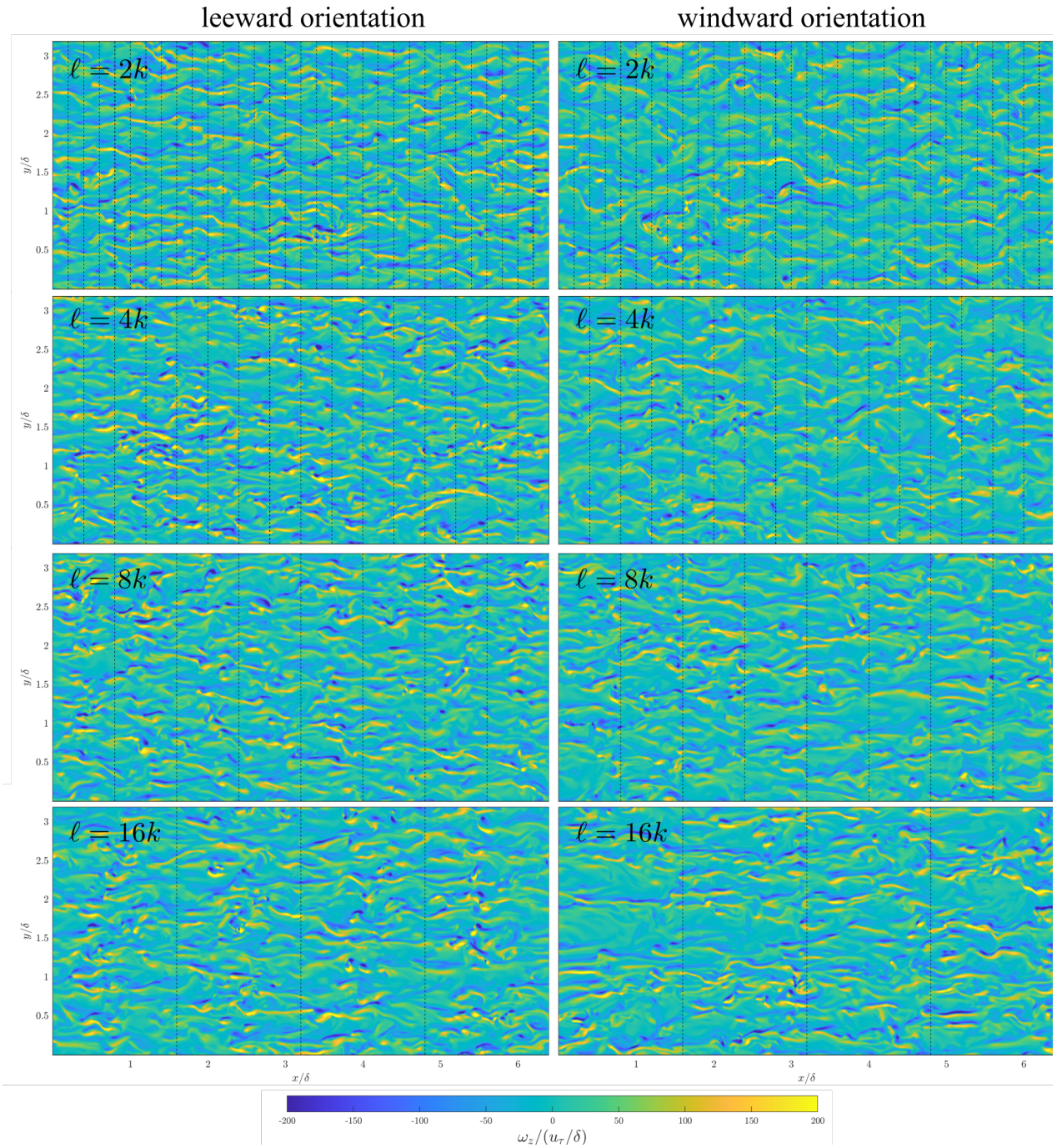

Figure 5. Structure of instantaneous ω_z at approximately 12 wall units above the roughness crest for ratchets with length $\ell = 2k$, $4k$, $8k$, and $16k$ (from top to bottom) in leeward (left column) and windward (right column) orientation. The black dotted lines indicate the locations of the roughness crests.